applied sciences

MDPI

Article

Pentacoordinated Liquid Crystalline Zn(II) Complex Organized in Smectic Mesophase: Synthesis, Structural and Electrochemical Properties

Adelina A. Andelescu [1], Sorina Ilies (b. Motoc) [1], Carmen Cretu [1], Evelyn Popa [1], Sorin Marinescu [1], Benoît Heinrich [2], Florica Manea [3,*], Sorina Negrea [4,5], Bertrand Donnio [2] and Elisabeta I. Szerb [1,*]

[1] “Coriolan Drăgulescu” Institute of Chemistry, Romanian Academy, 24 Mihai Viteazu Bvd., 300223 Timisoara, Romania
[2] Institut de Physique et Chimie des Matériaux de Strasbourg (IPCMS), UMR7504, CNRS-Université de Strasbourg, 67034 Strasbourg, France
[3] Department of Applied Chemistry and Engineering of Inorganic Compounds and Environment, Politehnica University of Timisoara, Blv. Vasile Parvan No. 6, 300223 Timisoara, Romania
[4] National Institute of Research and Development for Industrial Ecology (INCD ECOIND), Timisoara Branch, 300431 Timisoara, Romania
[5] Department of Environmental Engineering and Management, “Gheorghe Asachi” Technical University of Iasi, 700050 Iasi, Romania
* Correspondence: florica.manea@upt.ro (F.M.); eszerb@acad-icht.tm.edu.ro (E.I.S.)

Featured Application: The study was conducted as fundamental research aiming new advanced materials characterized envisaging applications of non-enzymatic electrochemical sensing.

Abstract: The synthesis and structural characterization of a new liquid crystalline coordination complex based on pentacoordinated Zn(II) metal centre with the coordination fulfilled by the tridentate chelating N^N^N 2,2′;6′,2′′-terpyridine ligand and two monoanionic gallates decorated with several long alkyl chains is described. The mesomorphic properties were accurately investigated by small- and wide-angle X-ray scattering studies. Despite the bulky coordination around the metal centre, the complex self-organizes into a smectic phase and, based on the structural and geometrical parameters, a model for the supramolecular organization in the liquid crystalline phase is proposed. Electrochemical investigations showed the importance of the molecular structure of the coordination complex in enhancing its aqueous sensing capacities: the bulky organic ligands form an organic shell separating the metal centres and favouring the redox system through their reduction followed by stripping.

Keywords: Zn(II) coordination complexes; metallomesogens; SWAXS; electrochemistry; nanoelectrodes assembly

check for updates

Citation: Andelescu, A.A.; Ilies (b. Motoc), S.; Cretu, C.; Popa, E.; Marinescu, S.; Heinrich, B.; Manea, F.; Negrea, S.; Donnio, B.; Szerb, E.I. Pentacoordinated Liquid Crystalline Zn(II) Complex Organized in Smectic Mesophase: Synthesis, Structural and Electrochemical Properties. *Appl. Sci.* **2022**, *12*, 8306. https://doi.org/10.3390/app12168306

Academic Editor: Marco Anni

Received: 22 July 2022
Accepted: 16 August 2022
Published: 19 August 2022

1. Introduction

Coordination complexes based on d-block metal centres are considered as promising molecular materials for bringing important advancements in applicative fields, such as opto-electronics, photonics, data storage, catalysis, biomedicine, etc., due to unique features imparted by the different nature of the molecular fragments, which, when combined together, contribute to the collective properties of the final material [1–10]. The redox, magnetic, optical, catalytic, electrical or electrochemical properties of the d-block metal ion centre can cooperatively interact with those of the organic ligands (redox, optic, biologic properties) and/or counterions (solubility in polar solvents, anion coordination) in the case of ionic species, to enhance or modify the overall properties of the architectural ensemble [11–19]. Indeed, the properties of a d-block-based metal coordination complex are more than the sum of the individual component's properties, and in many cases, synergistic unique physicochemical properties may be engineered this way [4,5,20], while the supramolecular arrangement is important due to the sensitivity of the coordination complex to the molecular surroundings, particularly for emission properties [21,22]. Thus, different soft or crystalline supramolecular architectures built up with the same "d-block metal containing building block" through non-covalent interactions can have varied photophysical properties, and small changes in their molecular structure may induce a huge modification of the materials response to external stimuli [5,15,16,21,22].

Zn(II)-based metallomesogens were mainly designed for application in electro-optics, due to the possibility of obtaining luminescent polarized emission [23–28]. Recently, a series of pentacoordinated Zn(II) coordination complexes (**Zn_1–4** in Figure 1) self-assembling into 2D hexagonal columnar and 3D mesophases was reported [27,28]. The symmetry of the mesophases was somehow expected taking into account the bulky coordination sphere around the Zn(II) ion fulfilled by a tridentate chelating N^N^N terpyridine (tpy) ligand differently substituted in apical position and two monoanionic gallate-based ligands. Indeed, the majority of tetra-, penta- and hexa-coordinated Zn(II) derivatives displayed columnar mesophases [24–34]; however, some smectic phases [23,35–38] or lamello-columnar phases were also reported [39].

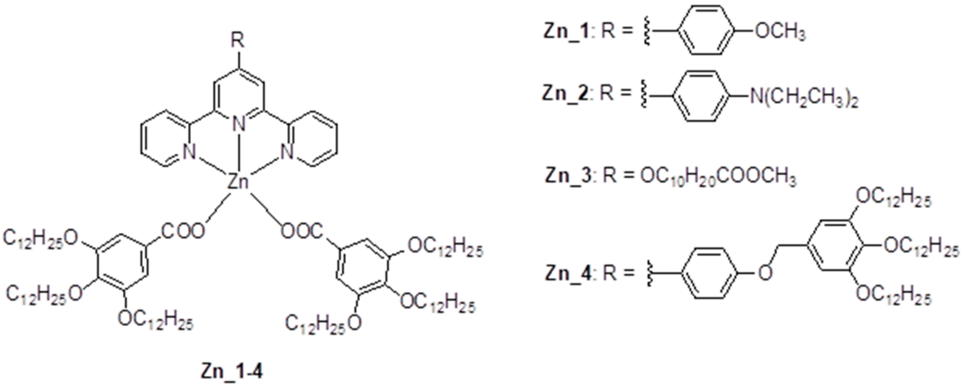

Figure 1. Chemical structure of the Zn(II) coordination complexes previously reported [27,28].

The monoanionic ligands decorated with several long alkyl chains were responsible for the induction of liquid crystalline properties, while the terpyridine-based substituents ($-C_6H_4R$, Figure 1) influenced the supramolecular arrangement by the modification of the interface between antagonistic aromatic and alkyl chains segments and were the determining factor for the photophysical properties: the electron-donating $-NEt_2$ group originated an ILCT excited state and **Zn_2** reaching a record luminescence quantum yield in solution (95%).

In electrochemical sensing, the presence of a d-block metal centre brings redox properties, while the organic ligands may act as a separator of the metal centres avoiding close contacts and implicit agglomeration; the separation of the redox active centres may yield micro or even nano-electrode arrays/assemblies, increasing the sensing performances, especially for bioanalysis devices [40–42]. The electrocatalytic activities of various forms of zinc oxides have been studied for multiple applications, e.g., the oxygen reduction (ORR) reaction that play an important role in renewable energy technologies [43,44], water electrooxidation for the generation of hydrogen peroxide [45] and for electrochemical sensing of various biologically active compounds [46,47]. Additionally, metallomesogens based on the redox active Cu(I) metal centre showed potential in improving the electrocatalytic performances of carbon-based materials for detection of bioanalytes [48,49]. Hence, our aim was to study the electrochemical behaviour of related Zn(II) coordination complex as a function of the molecular structure. In order to reduce the workload in the synthesis of complexes, we employed the non-substituted 2,2′;6′,2′′-terpyridine to obtain **Zn_tpy** (Scheme 1) with a reduced molecular structure and followed the changes in the supramolecular arrangement in condensed states. The electrochemical properties of complex **Zn_tpy** were investigated and discussed as a function of molecular structure.

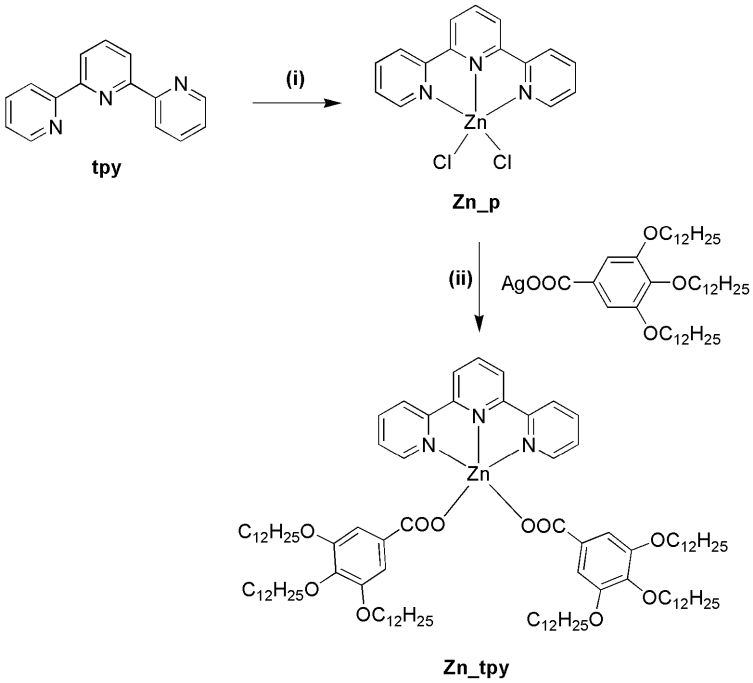

Scheme 1. Synthesis of **Zn_tpy**: (**i**) $ZnCl_2$, MeOH, r.t., 2 h; (**ii**) $CHCl_3$, r.t., 6 h.

2. Materials and Methods

The starting materials commercially available were used as received. The synthesis of the silver(I) salt of 3,4,5-tridodecyloxybenzoate was performed as reported in the literature [50]. ^{1}H and ^{13}C NMR experiments were recorded on Bruker Avance III HD–500 MHz spectrometer in CD_2Cl_2 or DMSO-d_6, using tetramethylsilane (TMS) as internal standard. Elemental analyses (CHN) were performed with a Flash 2000 microanalyzer from ThermoFisher Scientific. The percentage of Zn(II) was determined using a SensAA flame atomic absorption spectrometer (GBC Scientific Equipment, Australia) equipped with a zinc hollow cathode lamp (detection limit: 0.4–1.5 mg/L, wavelength: 213.9 nm, slit width: 0.5 nm). The flame used was an air–acetylene (oxidizing) mixture. Two determinations were made and the average absorbance value was further used.

Mesophases optical textures of complex **Zn_tpy** were observed with an Olympus BX53M polarizing microscope (POM) equipped with a Linkam hot stage. Images of the various phases were recorded using an Olympus UC90 camera. Enthalpies and transition temperatures were recorded using a Q1000 apparatus from TA Instruments. The apparatus was calibrated with indium; three heating/cooling cycles were performed on each sample, with a heating and cooling rate of 5 °C/min. Thermal gravimetric analysis (TGA) was carried out using a Q50 instrument from TA Instruments at a scanning rate of 5 °C/min and with air as purge gas.

S/WAXS patterns were obtained with a transmission Guinier-like geometry. A linear focalized monochromatic Cu Kα1 beam (λ = 1.5405 Å) was obtained using a sealed-tube generator (600 W) equipped with a bent quartz monochromator. In all cases, samples were filled in home-made sealed cells of 1 mm path. The patterns were recorded with a curved Inel CPS120 counter gas-filled detector linked to a data acquisition computer (periodicities up to 90 Å) and on image plates scanned by Amersham Typhoon IP with 25 µm resolution (periodicities up to 120 Å). The sample temperature was controlled within ±0.01 °C, and exposure times were varied from 2 to 6 h.

2.1. Synthesis

Complex **Zn_p**. A solution of $ZnCl_2$ (0.292 g, 2.143 mmol) in 10 mL of MeOH was added dropwise to a solution of ligand 2,2′;6′,2′′-terpyridine (0.500 g, 2.143 mmol) in 20 mL MeOH. During the addition of the Zn(II) salt, a pale-yellow precipitate formed. The reaction mixture was stirred for 2 h at r. t. Then, the yellowish precipitate was filtered off, washed with MeOH and dried under vacuum to yield 0.785 g (2.122 mmol, η = 99%) of the desired compound. FT-IR (KBr, cm^{-1}): 1594–1448 ($\upsilon_{C=C}$, $\upsilon_{C=N}$); ^{1}H-NMR (DMSO-d$_6$, δ/ppm): 8.82 (overlapped peaks, 4H), 8.60 (overlapped peaks, 3H), 8.34 (t, ^{3}J = 7.8 Hz, 2H), 7.86 (t, ^{3}J = 6.4 Hz, 2H). Anal. Calcd. for $C_{15}H_{11}Cl_2N_3Zn$ (369.56 g·mol^{-1}): C, 48.75; H, 3.00; N, 11.37. Found: C, 48.58; H, 3.06; N, 11.03%.

Complex **Zn_tpy**. A solution of Ag(I) salt of 3,4,5-tridodecyloxybenzoate (0.698 g, 0.893 mmol) in 25 mL $CHCl_3$ was added dropwise to a suspension of **Zn_p** (0.150 g, 0.4054 mmol) in 40 mL of $CHCl_3$. The reaction mixture was stirred at room temperature for 6 h. After the removal of AgCl by filtration, the mother liquor was evaporated under reduced pressure. The residue was dissolved in Et_2O and acetone was added. The precipitate formed was filtered out, and the pure product was obtained from the mother solution by repeated recrystallization from acetone and hexane/EtOH (0.315 g, η = 47%). FT-IR (KBr, cm^{-1}): 2924 (νas,(-CH$_{2-}$)), 2854 (νs,(-CH$_{2-}$)), 1623 (νas,(COO$^-$)), 1567–1428 ($\upsilon_{C=C}$, $\upsilon_{C=N}$) 1359 (νs(COO$^-$)); ^{1}H-NMR (CD_2Cl_2, δ/ppm): 8.87 (d, ^{3}J = 5.0 Hz, 2H), 8.20 (overlapped peaks, 5H), 7.96 (t, ^{3}J = 7.8 Hz, 2H), 7.49 (t, ^{3}J = 7.6 Hz, 4H), 7.09 (s, 2H), 3.83 (overlapped peaks, 12H), 1.77–1.26 (overlapped peaks, 120 H), 0.79 (t, ^{3}J = 6.8 Hz, 18H). Anal. Calcd. for $C_{101}H_{165}N_3O_{10}Zn$ (1646.79 g·mol^{-1}): C, 73.66; H, 10.10; N, 2.55. Found: C, 73.46; H, 10.05; N, 2.64%. AAS: Zn% calcd.: 3.97, found: 3.91.

2.2. Electrochemical Characterization

All electrochemical experiments were carried out in 0.1 M NaOH solutions by cyclic voltammetry (CV) technique in a three-electrode cell connected with an Autolab potentiostat/galvanostat PGSTAT 302 (EcoChemie, The Netherlands) controlled with GPES 4.9 software. The working electrode was a glassy carbon (**GC**) provided by Metrohm (Switzerland) with the disk diameter of 5.0 mm. The counter electrode was a platinum plate electrode with the geometrical surface area of 1.0 cm^2. The electrode potentials were recorded against saturated calomel reference (SCE) electrode. **GC** working electrode was modified with **Zn_tpy** and named **Zn_tpy/GC** electrode; its electrochemical behaviour was studied by comparison with simple **GC** electrode in 0.1 M NaOH supporting electrolyte. The **GC** electrode was mechanically cleaned by polishing with alumina, followed by rinsing with distilled water and drying. The modification was done by simple film casting through cleaned **GC** electrode immersion within a non-aqueous suspension containing 5 mg **Zn_tpy** /mL acetonitrile. After immersion, the electrode surface was dried at room temperature. All measurements were performed at room temperature (25 ± 1 °C).

3. Results and Discussion

3.1. Synthesis and Characterization

For the synthesis of the complex **Zn_tpy**, we employed the synthetic strategy previously reported, that requires first the synthesis of the dichloro Zn(II) precursor (**Zn_p** in Scheme 1), followed by its reaction with the Ag(I) salt of 3,4,5-tridodecyloxybenzoate [27,28]. The complex **Zn_tpy** was obtained by repeated crystallizations as a yellowish powder and was dried in vacuum for several hours. Structural characterizations were performed by FT-IR and ^{1}H NMR spectroscopies, while the purity was confirmed by elemental analysis and AAS spectroscopy (Supplementary Materials, Figure S1).

3.2. Thermal and Mesomorphic Properties

The thermal stability was determined by thermogravimetric analysis (TGA) (Supplementary materials, Figure S2), while the transition temperatures and the enthalpy changes associated were investigated by differential scanning calorimetry (DSC) (Supplementary materials, Figure S3). The data are presented in Table 1.

Table 1. Thermal and mesomorphic data for **Zn_tpy**.

$T_{dec5\%}$ [a] [°C]	Mesophases [b], Transition Temperatures (°C) and Enthalpies [ΔH (kJ·mol^{-1})] [c]
245	Cr 89 [12.0] SmA 109 [2.5] Isso/Isso 114 [2.6] SmA 73 [10.2] Sm + Cr

[a] Decomposition temperature at 5% weight-loss (from TGA); [b] SmA: smectic A mesophase; [c] DSC data on second heating and cooling cycles.

For **Zn_tpy**, weight-loss from degradation becomes significant above ca. 170 °C, with a 5% weight-loss at 230 °C (at a rate of 5 °C min^{-1}). Polarized optical microscopy investigations (POM) showed that, on cooling from the isotropic liquid, the complex self-assembles into a liquid crystalline mesophase (Figure 2a) below 114 °C, as indicated by the growth of a fan-shaped, fluid but non-characteristic, optical texture. The final identification of the type and symmetry of the mesophase was achieved by small- and wide-angle X-ray scattering studies (S/WAXS–Figure 2b, Supplementary materials, Figure S4).

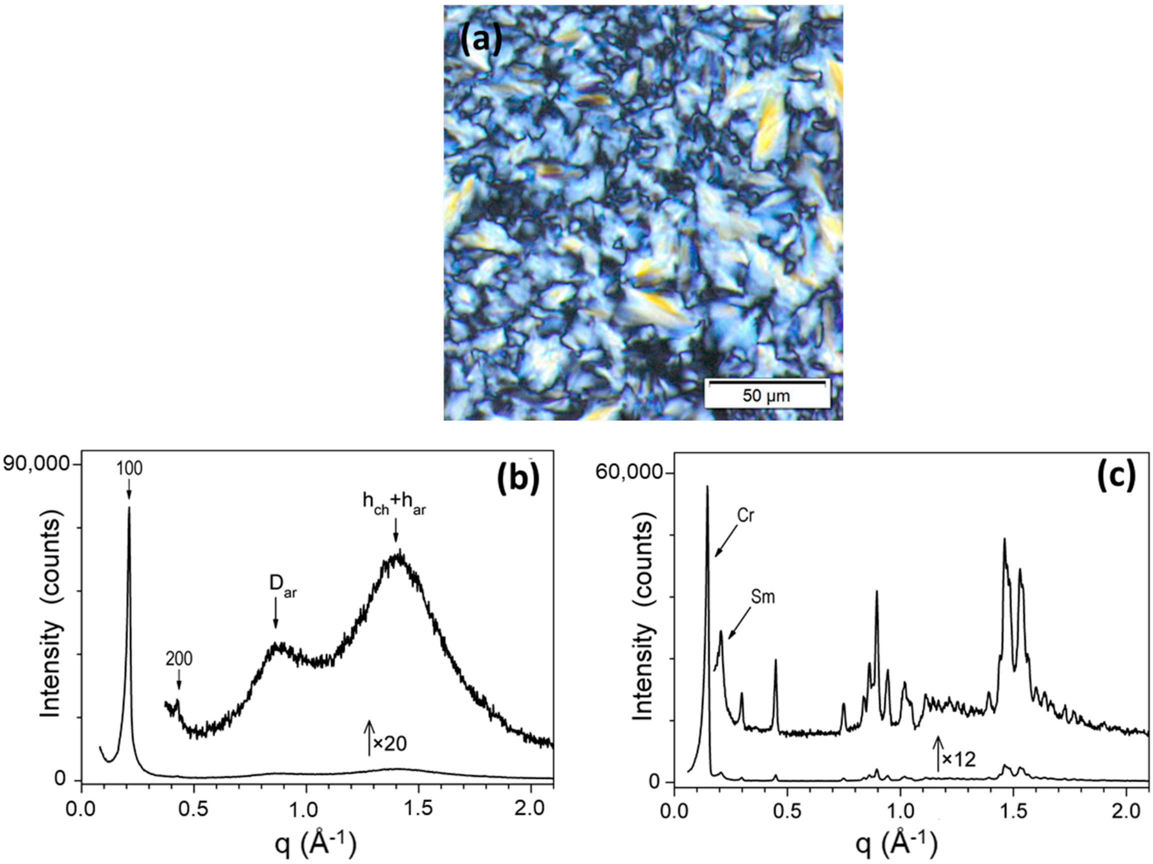

Figure 2. (**a**) POM texture of **Zn_tpy** on cooling at 110 °C, magnification 20×; SWAXS patterns of **Zn_tpy;** (**b**) at 85 °C in the mesophase and (**c**) at room temperature in the pasty pseudo-crystalline state, showing coexistence of the signals of the crystal phase and smectic A phase.

The SWAXS patterns are typical of a liquid crystalline smectic phase, with the overlapping broad scattering signal arising from liquid-like lateral distances between undifferentiated molecular segments, i.e., molten chains, h_{ch}, and aromatic parts, har, in the wide-angle region (h_{ch} + h_{ar}), and with two sharp small-angle reflections corresponding to the first two lamellar orders (h00) (100, very strong, and 200, weak), emerging from the nanosegregated structure formed by the antagonistic aromatic and aliphatic segments (Figure 2b); an additional broad signal, corresponding to short-range periodicity from the arrangement of the metallic-tpy moiety within aromatic layers, D_{ar}, was also observed at ca. 7.5–8.0 Å.

Due to the specific amphiphilic molecular structure of the zinc complex, with the six alkyl chains radiating in the same direction, whereas the tpy moiety is deprived of chains, the complexes are probably self-organized pairwise in a more or less head-to-head fashion (Figure 3), with the aromatic and metallic moieties confined into a median sublayer (D_{ar}), whose periodic alternation with molten chain sublayers generates a SmA-like structure with a periodicity d_{lam} of ca. 29.3 Å at 85 °C (ca. 28.9 Å at 100 °C, Table 2).

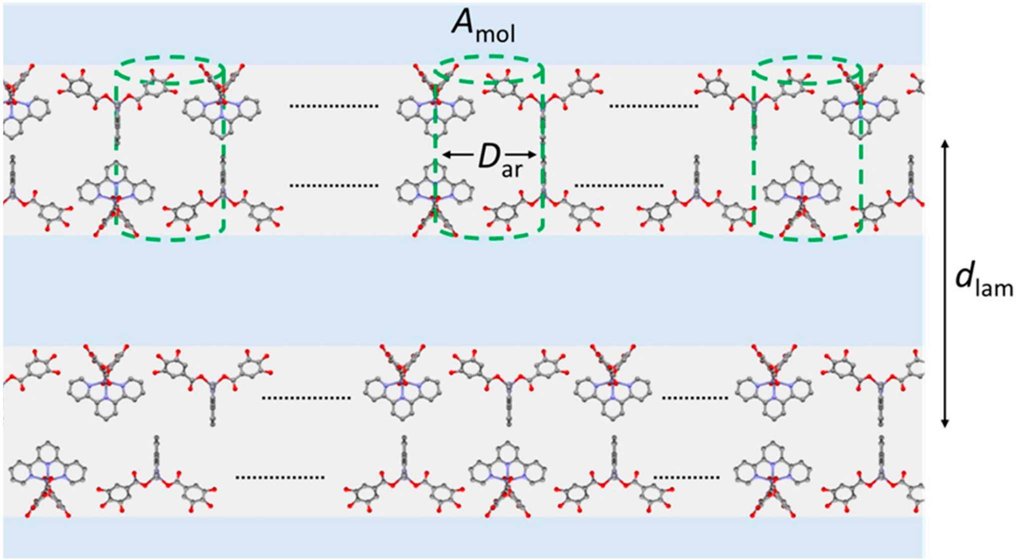

Figure 3. Idealized supramolecular representation of the **Zn_tpy** complexes in the SmA phase through self-assembly of aromatic and metallic moieties into monolayers (various possibilities of head-to-head arrangements are shown, with, in some cases, the possibility of larger interdigitation) alternating with molten chains (aliphatic chains continuum is shown in pale blue); d_{lam} and A_{mol} are the lamellar periodicity and molecular area, and Dar is the average separation between [**Zn_tpy**] moieties, $D_{ar} \sim \sqrt{(A_{mol}/\pi)}$ (see Table 2).

Table 2. Geometrical mesophases parameters.

Sample Phase, T	Vmol ρ	d_{lam}	N_{molL} A_{mol}	N_{arL} S_{ZnAr}	N_{chL} S_{ch}	q_{ch}
Zn_tpy SmA, 85	27,530.99	29.31	2 188	1 94	2 31.3	1.41
Zn_tpy SmA, 100	2781 0.98	28.89	2 192	1 96	2 32.1	1.43

T, temperature of the measurement (°C); Vmol, calculated molecular volume (Å^3); ρ, density (g/cm^3); d_{lam}, lamellar periodicity (Å); N_{molL}, number of molecular layers per lamella; $A_{mol} = N_{molL} \times V_{mol}/d$, molecular area (Å^2); N_{arL}, number of aromatic layers per lamella ($N_{arL} = 1$ for monolayer arrangement); $S_{ZnAr} = (N_{arL}/N_{molL}) \times A_{mol}$, surface per Zinc complex (Å^2); N_{chL}, number of chain layers per lamella ($N_{chL} = 2$ for non-interdigitated chains); $S_{ch} = (N_{chL}/N_{molL}) \times A_{mol}/n_{ch}$, surface per chain (Å^2), $n_{ch} = 6$ being the number of peripheral chains per molecule; $q_{ch} = S_{ch}/\sigma_{ch}$, chain packing ratio, $\sigma_{ch} = (26.5616 + 0.02023T)/1.27$ (Å^2) being the cross-sectional area of a molten chain [51].

The geometry of the Zn complexes can be deduced from the single-crystal structures of molecules, including the same complex moiety. In this way, structures of several Zinc bis(enzoate)-phenylterpyridine derivatives are available (CSD-BETWOO, CSD-BETWUU, CSD-BETXAB, CSD-LEXWES) [52] and show irregular trigonal bipyramidal geometries, in which both benzoate ligands are nearly orthogonal to the terpyridine ring plane.

In **Zn_tpy**, benzoate ligands consist of gallate units substituted by three long dodecyl chains, whose rejection into adjacent molten aliphatic layers generates a smectic A-like organization (Figure 3). The formation of such lamellar structure implies that the molecular packing within the aromatic layer matches the high overall cross-sectional area of the six pending chains ($6 \times \sigma_{ch} \approx 135$ Å^2). This condition is realized through a monolayer configuration alternating terpyridine rings and gallate segments in the layer plane. This arrangement, which is also found in CSD-BETWOO and otherwise explains the in-plane periodicity Dar, offers a high molecular cross-section ($S_{ZnAr} = 87$ Å^2 in CSD-BETWOO and $S_{ZnAr} \approx 95$ Å^2 in **Zn_tpy**, Table 2). Above all, it allows sharing alkyl substituents between both adjacent layers, and thus elevates the molecular area to $A_{mol} \approx 190$ Å^2, which even exceeds the requirement for alkyl chains (q_{ch}). This discrepancy is, however, easily compensated by a higher degree of the folding of the chains, to the cost of more diffuse interfaces and of a lower efficient nanosegregation between antagonistic moieties. This effect should contribute to the narrowness of the smectic range and to the difficulty to detect the lamellar higher order reflections.

The reduction of the molecular structure beside easing the synthesis has a significant influence on the supramolecular organisation in the mesophase: the non-substituted coordination complex described herein **Zn_tpy**, arranges into smectic phases while the apical substitution of the tpy ligand direct the self-assembly into room temperature hexagonal mesophases, as previously reported for **Zn_1-4** [27,28] (Figure 1). Indeed, depending on the functionality of the tpy substituent, the complexes self-assemble either into 3D hexagonal mesophase (M_{hex}) or in 2D hexagonal lattice (Col_h) (See Figure 4).

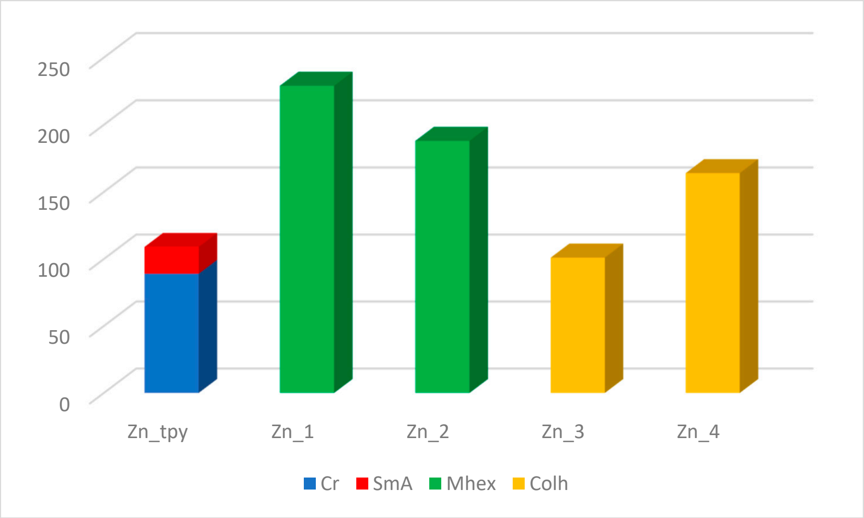

Figure 4. Mesomorphic behaviour of Zn(II) coordination complexes: Cr—crystalline phase; SmA—smectic A mesophase; M_{hex}—three-dimensional mesophase with a two-dimensional hexagonal lattice symmetry, Col_h: two-dimensional columnar hexagonal mesophase. DSC data on the second cooling cycle.

3.3. Electrochemistry

Studies regarding the electrochemical behaviour of functional materials, such as metallomesogens, are mandatory for any type of electrochemical application, such as electrochemical sensing. CV technique is a valuable tool to understand the processes that occur at the electrode surface containing a liquid crystal. However, the electrode composition cannot only contain the metallomesogen because it is not able to ensure the electrical conductivity suitable for electrochemical applications, but it can be used as modifier for the carbon-based electrode to enhance its electrochemical properties. In this study, the **GC** electrode was used as a substrate and **Zn_tpy** as a modifier, resulting in a **Zn_tpy/GC** electrode. In order to evaluate the importance of the molecular structure on the electrochemical performance of the modified **GC** electrode, the electrode was characterized in comparison with a **GC** electrode modified with the dichloro Zn(II) precursor **Zn_p** (Scheme 1), which lacks alkyl chains yielding electrode **Zn_p/GC,** and with a simple unmodified **GC** electrode. The electrochemical behaviour was studied in 0.1 M NaOH and attempted to reach zinc oxide species, which exhibited enhanced electrocatalytic activity for the electrooxidation processes.

The comparative cyclic voltammograms of the **GC** electrode, **Zn_p/GC** electrode and **Zn_tpy/GC** electrode in 0.1 M NaOH are presented in Figure 5.

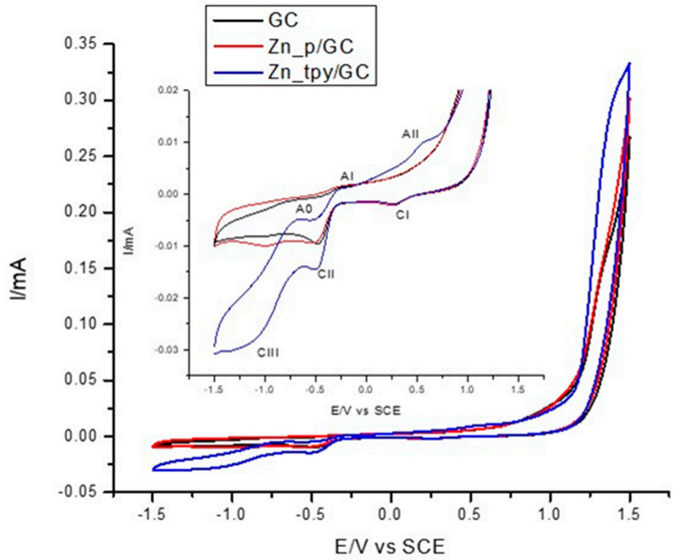

Figure 5. Cyclic voltammograms recorded in 0.1 M NaOH supporting electrolyte at a scan rate of 0.05 V·s^{-1} with **GC** electrode (black line), **Zn_p/GC** (red line) and **Zn_tpy/GC** electrode (blue line) within the potential range of −1.5 to +1.5 V/SCE; Inset: details of CVs, including the anodic and cathodic peaks marking.

CV shape recorded at **GC** electrode is changed significantly by the presence of **Zn_tpy** onto the **GC** electrode vs. the **Zn_p** presence onto the electrode that influences negligibly the negative cathodic range in comparison with **GC**. This means that no electrochemical behaviour is manifested by **Zn_p** to be considered as redox systems for further involvement within oxidation and reduction electrode processes. First of all, to understand the electrochemical behaviour of **Zn_tpy**, it is important to identify all processes that occurred onto **GC** electrode in 0.1 M NaOH. By forward scanning, starting from −1.50 V vs. SCE, an anodic peak (AI) is evidenced at the potential value of about −0.25 V vs. SCE, and at the potential value of about +1.00 V vs. SCE, the oxygen evolution reaction (OER) occurred with a low shoulder type anodic peak at about +1.25 V, which is characterised by the diffusion-controlled oxygen evolution in alkaline medium of carbon-based electrodes. The first anodic peak should be attributed to the oxidation of the easily oxidizable functional groups of the **GC** surface [53]. By reverse scanning, three cathodic peaks (CI-CIII, Figure 5) appeared on the **GC** electrode. CI recorded at the potential value of +0.26 V vs. SCE is usually attributed to the reduction of H_2O and/or dissolved O_2 that is well-known as the oxygen reduction reaction (ORR). However, in accordance with the literature data [54], this peak can be attributed to the reduction of difficult oxidized surface functional groups (e.g., edge or basal hydroxyl sites). Considering the high anodic potentials corresponding to OER, the produced oxygen can be divided into inner (adsorbed or trapped onto electrode surface) and dissolved outer oxygen. The appearance of CII and CIII cathodic peaks at −0.50 V and −1.00 V vs. SCE are ascribed to the reduction of the inner and dissolved outer O_2, which could occur by 4-electron pathway (reaction 1) and two successive 2-electron pathways, according to the reactions (reactions 2 and 3):

$$O_2 + 2H_2O + 4e^- \rightarrow 4HO^- \quad (1)$$

$$O_2 + H_2O + 2e^- \rightarrow HO_2^- + HO^- \quad (2)$$

$$HO_2{}^- + H_2O + 2e^- \rightarrow 3HO^- \tag{3}$$

Moreover, under the potential range of CIII, the hydrogen evolution reaction (HER) occurred onto **GC** electrode, which is partially overlapping with ORR.

All cathodic and anodic peaks were influenced by the presence of **Zn_tpy**. Thus, a slight polarization effect towards the OER is noticed and the shoulder recorded at +1.25 V/SCE is higher due to zinc oxide dissolution overlapping with O_2 evolution. Considering the literature data related to zinc deposition and zinc oxide formation [55–57], during cathodic direction scanning, starting with −0.760 V, metallic zinc is deposited, which can continue at more negative potentials than −1.5 V vs. SCE. Moreover, under this negative potential range of ORR, ZnO can be formed based on EC (electrochemical/chemical) mechanism by coupling the zinc ions with peroxide and superoxide ions, which are generated from oxygen reduction reaction, according with reactions (4 and 5):

$$Zn^{2+} + O_2{}^{2-} \rightarrow ZnO_2 \rightarrow ZnO + \frac{1}{2}{}^{o}{}_2 \tag{4}$$

$$Zn^{2+} + 2{}^{o}{}_2{}^- \rightarrow ZnO_4 \rightarrow ZnO + 3/2{}^{o}{}_2 \tag{5}$$

These processes are proved by the CII cathodic peak increasing, which is related with the anodic peak from +1.25 V/SCE, considering both the higher concentrations of Zn^{2+} and ORR products.

Another alternative considers the conversion of metallic zinc deposit into ZnO through peroxide ions generated by ORR, based on reaction (6):

$$Zn + \frac{1}{2}O_2{}^{2-} \rightarrow ZnO + 1e^- \tag{6}$$

This process occurred at a more negative potential, at which zinc ions are reduced to metallic deposits that can be oxidized via peroxide generated from ORR, which is evidenced by CIII cathodic peak increasing. During anodic scanning, the first anodic peak (A0) appeared only in the presence of **Zn_tpy** at about −0.55 V vs. SCE, being a characteristic feature of the stripping of Zn deposited onto a GC electrode. At more positive scanning, the AI anodic peak increased due to the dissolution of metallic zinc and zinc oxide. A new anodic peak is evidenced at the potential value of about +0.65 V vs. SCE (A II), which can be attributed to the zinc oxide dissolution with the zincate formation (reaction (7)), which is controlled by the HO^- anions diffusion at the electrode surface.

$$ZnO + H_2O + 2HO^- \rightarrow Zn(OH)_4{}^{2-} \tag{7}$$

To further elucidate several mechanistic aspects, the influence of the scan rate on CV shape recorded at **Zn_tpy/GC** electrode was studied. The family of CVs recorded for the scan rate, ranged between 0.01 to 0.20 $V{\cdot}s^{-1}$, are presented in Figure 6. When the scan rate is ranged from 0.01 to 0.10 $V{\cdot}s^{-1}$, the usual behaviour characteristics to the diffusion-controlled processes is observed for all cathodic and anodic peaks. However, the negative and low current of the A0 anodic peak was noticed, which did not vary linearly with the scan rate that informed us about the slow rate and the electron transfers-controlled process at the beginning of zinc stripping from zinc deposited onto the **GC** electrode. Moreover, the currents corresponding to the CIII cathodic peak linearly increased with the scan rate, which means the diffusion-controlled overall process of metallic zinc deposition and more overlapped cathodic processes, including hydrogen evolution. The linear dependences of the cathodic and anodic peaks currents with the square root of the scan rates are presented in Figure 7a, and all the ORR and zinc and zinc oxide stripping at more positive potentials are diffusion-controlled.

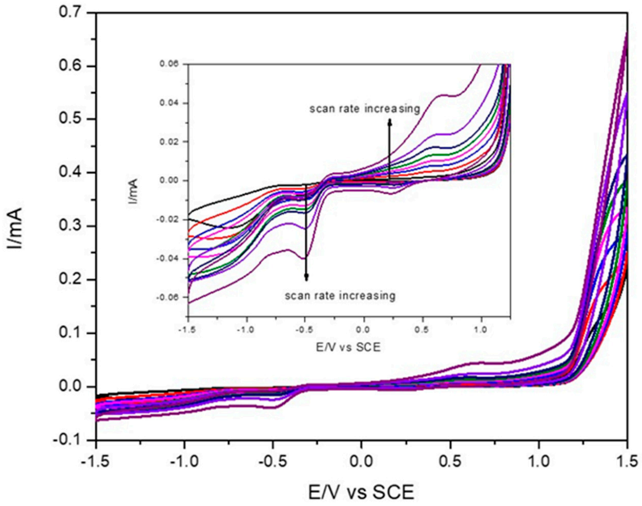

Figure 6. CVs recorded at **Zn_tpy/GC** electrode in 0.1 M NaOH supporting electrolyte at various scan rates of: 0.01; 0.02; 0.03; 0.05; 0.06; 0.1; 0.2 V·s^{-1} (curves 1–8) within potential range from −1.5 V to +1.5 V vs. SCE.

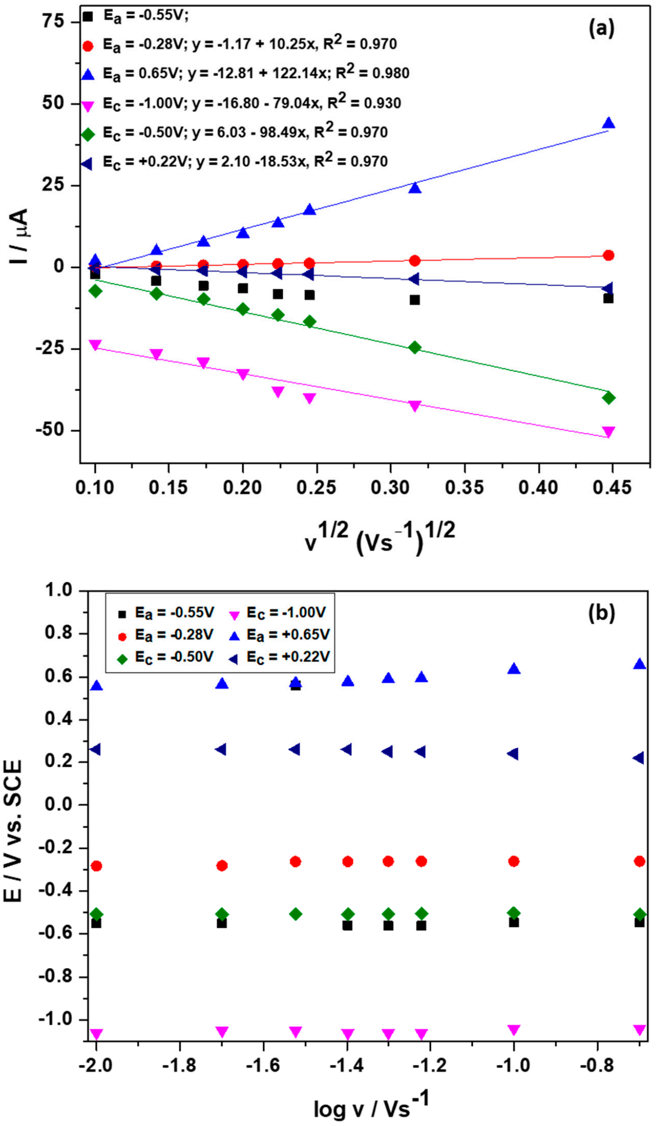

Figure 7. (**a**) Linear dependence of the peaks currents vs. square root of the scan rate; (**b**) Dependence of the peak potentials vs. the logarithm of the scan rate.

Very slight shifting of the oxidation and reduction peak potentials is found (Figure 7b), being practically independent of the voltammetry timescale, which informed us about the steady-state cathodic and anodic processes on the **Zn_tpy/GC** electrode.

4. Conclusions

A new metallomesogen based on a pentacoordinated Zn(II) metal centre was synthesized and characterized. Despite its bulky coordination, the coordination complex arranged into smectic layers starting from 89 °C. On cooling, the smectic phase is retained at room temperature and found to co-exist with the crystalline phase. An arrangement in the smectic phase is proposed based on X-ray scattering studies at both small- and wide-angles.

The electrochemical behaviour of the amphiphilic complex **Zn_tpy,** as a modifier of the **GC** electrode, was studied in comparison with its precursor **Zn_p** that lacks alkyl chains. The amphiphilic structure of the metallomesogen confers special properties for the complex regarding its electrochemical behaviour. The anodic and cathodic peaks identified for **Zn_tpy/GC** electrode in 0.1 M NaOH supporting electrolyte using cyclic voltammetry revealed the presence of redox systems for the whole potential range from −1.5 to +1.5 V vs. SCE. Within the negative potential range, the metallic zinc deposition and zinc oxide formation occurred during cathodic scanning at a potential value more negative than −0.55 V vs. SCE and zinc stripping was identified at a higher potential value. At a more positive potential range, higher than +0.65 V vs. SCE, the zinc oxide dissolution with the zincate formation controlled by the HO^- anions diffusion at the electrode surface occurred, which is overlapped at about +1.25 V vs. SCE with oxygen evolution reaction. This behaviour makes this complex suitable to be used in electrode modification/functionalization to confer it electrocatalytic activity vs. its dichloro precursor **Zn_p** that did not exhibit redox systems. The differences may derive from the different molecular structure of the two complexes; while in the case of **Zn_p** there is more likely a closer vicinity of the metal centres and their unavailability for involvement in the reduction and oxidation electrode processes, in the case of **Zn_tpy**, the bulky gallate ligands form an organic shell that keeps the metal centres more or less isolated, not permitting close contacts, which make them available for Zn reduction followed by its stripping. This can be a strategy to build performant sensing materials with nanoseparated electrochemically active centres.

Supplementary Materials: The following supporting information can be downloaded at: https://www.mdpi.com/article/10.3390/app12168306/s1, Figure S1: ^{1}H NMR spectra of complex **Zn_tpy**; Figure S2: TGA trace of complex **Zn_tpy**; Figure S3: DSC trace of complex **Zn_tpy**; Figure S4: S/WAXS pattern of complex **Zn_tpy** at 100 °C.

Author Contributions: Conceptualization, B.D., F.M. and E.I.S.; methodology, E.I.S.; investigation, B.H., A.A.A., E.P., S.M., S.I., S.N., C.C.; resources, E.I.S.; data curation, B.D., F.M. and E.I.S.; writing—original draft B.D., F.M. and E.I.S. and E.I.S.; writing—review and editing, B.D., F.M. and E.I.S. All authors have read and agreed to the published version of the manuscript.

Funding: This work was supported by a grant of the Romanian Ministry of Education and Research, CNCS-UEFISCDI, project number PN-III-P4-ID-PCE-2020-1958, within PNCDI III.

Institutional Review Board Statement: Not applicable.

Informed Consent Statement: Not applicable.

Data Availability Statement: Not applicable.

Acknowledgments: We acknowledge the Romanian Academy, Program 4 and B.D. and B.H. thank CNRS and University of Strasbourg for support. This work was supported by a grant of the Ministry of Research, Innovation and Digitization, CNCS/CCCDI–UEFISCDI, project number PN-III-P4-ID-PCE-2020-1958, within PNCDI III.

Conflicts of Interest: The authors declare no conflict of interest.

References

1. Housecroft, C.E.; Constable, E.C. Solar energy conversion using first row d-block metal coordination compound sensitizers and redox mediators. *Chem. Sci.* **2022**, *13*, 1225–1262. [CrossRef]
2. Bozic-Weber, B.; Constable, E.C.; Housecroft, C.E. Light harvesting with Earth abundant d-block metals: Development of sensitizers in dye-sensitized solar cells (DSCs). *Coord. Chem. Rev.* **2013**, *257*, 3089–3106. [CrossRef]
3. Howarth, A.J.; Majewski, M.B.; Wolf, M.O. Photophysical properties and applications of coordination complexes incorporating pyrene. *Coord. Chem. Rev.* **2015**, *282*, 139–149. [CrossRef]
4. Greenfield, T.J.; Julve, M.; Doyle, R.P. Exploring the biological, catalytic, and magnetic properties of transition metal coordination complexes incorporating pyrophosphate. *Coord. Chem. Rev.* **2019**, *384*, 37–64. [CrossRef]
5. Pan, M.; Liao, W.-M.; Yin, S.-Y.; Sun, S.-S.; Su, C.-Y. Single-Phase White-Light-Emitting and Photoluminescent Color-Tuning Coordination Assemblies. *Chem. Rev.* **2018**, *118*, 8889–8935. [CrossRef]
6. Kumar, N.; Bhalla, V.; Kumar, M. Beyond zinc coordination: Bioimaging applications of Zn(II)-complexes. *Coord. Chem. Rev.* **2021**, *427*, 213550. [CrossRef]
7. Gupta, D.; Sathiyendiran, M. Rhenium-Carbonyl-Based Supramolecular Coordination Complexes: Synthesis, Structure and Properties. *Chem. Sel.* **2018**, *3*, 7439–7458. [CrossRef]
8. Cargnelutti, R.; Schumacher, R.F.; Belladona, A.L.; Kazmierczak, J.C. Coordination chemistry and synthetic approaches of pyridyl-selenium ligands: A decade update. *Coord. Chem. Rev.* **2021**, *426*, 213537. [CrossRef]
9. Marchetti, F.; Pettinari, C.; Di Nicola, C.; Tombesi, A.; Pettinari, R. Coordination chemistry of pyrazolone-based ligands and applications of their metal complexes. *Coord. Chem. Rev.* **2019**, *401*, 213069. [CrossRef]
10. Malinowski, J.; Zych, D.; Jacewicz, D.; Gawdzik, B.; Drzezdzon, J. Application of Coordination Compounds with Transition Metal Ions in the Chemical Industry—A Review. *Int. J. Mol. Sci.* **2020**, *21*, 5443. [CrossRef]
11. Chalkley, M.J.; Drover, M.W.; Peters, J.C. Catalytic N_2-to-NH_3 (or -N_2H_4) Conversion by Well-Defined Molecular Coordination Complexes. *Chem. Rev.* **2020**, *120*, 5582–5636. [CrossRef] [PubMed]
12. Chylewska, A.; Biedulska, M.; Sumczynski, P.; Makowski, M. Metallopharmaceuticals in Therapy—A New Horizon for Scientific Research. *Curr. Med. Chem.* **2018**, *25*, 1729–1791. [CrossRef]
13. Pervaiz, M.; Sadiq, S.; Sadiq, A.; Younas, U.; Ashraf, A.; Saeed, Z.; Zuber, M.; Adnan, A. Azo-Schiff base derivatives of transition metal complexes as antimicrobial agents. *Coord. Chem. Rev.* **2021**, *447*, 214128. [CrossRef]
14. Doistau, B.; Jimenez, J.R.; Piguet, C. Beyond Chiral Organic (p-block) Chromophores for Circularly Polarized Luminescence: The Success of d-Block and f-Block Chiral Complexes. *Front. Chem.* **2020**, *8*, 555. [CrossRef] [PubMed]
15. Maiuolo, L.; Calandra, P.; Lombardo, D.; Szerb, E.I. Amphiphiles-metals interactions for applications in modern technologies: Recent developments and future perspectives. *Rev. Roum. Chim.* **2020**, *65*, 647–671. [CrossRef]
16. Cretu, C.; Maiuolo, L.; Lombardo, D.; Szerb, E.I.; Calandra, P. Luminescent Supramolecular Nano- or Microstructures Formed in Aqueous Media by Amphiphile-Noble Metal Complexes. *J. Nanomater.* **2020**, *2020*, 5395048. [CrossRef]
17. Pellei, M.; Del Bello, F.; Porchia, M.; Santini, C. Zinc coordination complexes as anticancer agents. *Coord. Chem. Rev.* **2021**, *445*, 214088. [CrossRef]
18. Yang, D.; Zhao, J.; Yang, X.-J.; Wu, B. Anion-coordination-directed self-assemblies. *Org. Chem. Front.* **2018**, *5*, 662–690. [CrossRef]
19. Kameo, H.; Nakazawa, H. Recent Developments in the Coordination Chemistry of Multidentate Ligands Featuring a Boron Moiety. *Chem. Asian J.* **2013**, *8*, 1720–1734. [CrossRef]
20. Zhang, X.; Hou, Y.; Xiao, X.; Chen, X.; Hu, M.; Geng, X.; Wang, Z.; Zhao, J. Recent development of the transition metal complexes showing strong absorption of visible light and long-lived triplet excited state: From molecular structure design to photophysical properties and applications. *Coord. Chem. Rev.* **2020**, *417*, 21337. [CrossRef]
21. Dey, N.; Haynes, C.J.E. Supramolecular Coordination Complexes as Optical Biosensors. *Chem. Plus Chem.* **2021**, *86*, 418–433. [CrossRef] [PubMed]
22. Cuerva, C.; Cano, M.; Lodeiro, C. Advanced Functional Luminescent Metallomesogens: The Key Role of the Metal Center. *Chem. Rev.* **2021**, *121*, 12966–13010. [CrossRef]
23. Pastor, M.J.; Cuerva, C.; Fernández-Lodeiro, A.; Lodeiro, C.; Campo, J.A.; Cano, M. Designing Zn(II) complexes as a support of bifunctional liquid crystal and luminescent materials. *Dyes Pigm.* **2018**, *149*, 37–50. [CrossRef]
24. Chakraborty, S.; Mondal, P.; Prasad, S.K.; Rao, D.S.S.; Bhattacharjee, C.R. Zinc(II)-salphen complexes bearing long alkoxy side arms: Synthesis, solvent dependent aggregation, and spacer group substituent effect on mesomorphism and photophysical property. *J. Molec. Liq.* **2017**, *246*, 290–301. [CrossRef]
25. Chakraborty, S.; Mondal, P.; Prasad, S.K.; Rao, D.S.S.; Bhattacharjee, C.R. Induction of Mesomorphism through Supramolecular Assembly in Metal Coordination Compounds of "salphen"-Type Schiff Bases: Photoluminescence and Solvatochromism. *Eur. J. Inorg. Chem.* **2016**, *28*, 4604–4614. [CrossRef]
26. Kumar, N.S.S.; Shafikov, M.Z.; Whitwood, A.C.; Donnio, B.; Karadakov, P.B.; Kozhevnikov, V.N.; Bruce, D.W. Mesomorphism and Photophysics of Some Metallomesogens Based on Hexasubstituted 2,2′:6′, 2″-Terpyridines. *Chem. Eur. J.* **2016**, *22*, 8215–8233. [CrossRef] [PubMed]
27. Andelescu, A.A.; Heinrich, B.; Spirache, M.A.; Voirin, E.; La Deda, M.; Di Maio, G.; Szerb, E.I.; Donnio, B.; Costisor, O. Playing with PtII and ZnII Coordination to Obtain Luminescent Metallomesogens. *Chem. Eur. J.* **2020**, *26*, 4850–4860. [CrossRef]

28. La Deda, M.; Di Maio, G.; Candreva, A.; Heinrich, B.; Andelescu, A.A.; Popa, E.; Voirin, E.; Badea, V.; Amati, M.; Costisor, O.; et al. Very intense polarized emission in self-assembled room temperature metallomesogens based on Zn(II) coordination complexes: An experimental and computational study. *J. Mater. Chem. C* **2022**, *10*, 115–125. [CrossRef]
29. Cavero, E.; Uriel, S.; Romero, P.; Serrano, J.L.; Giménez, R. Tetrahedral Zinc Complexes with Liquid Crystalline and Luminescent Properties: Interplay Between Nonconventional Molecular Shapes and Supramolecular Mesomorphic Order. *J. Am. Chem. Soc.* **2007**, *129*, 11608–11618. [CrossRef]
30. Pucci, D.; Crispini, A.; Ghedini, M.; La Deda, M.; Liguori, P.F.; Pettinari, C.; Szerb, E.I. "Green light" for Zn(II) mesogens. *RSC Adv.* **2012**, *2*, 9071–9078. [CrossRef]
31. Keerthiga, R.; Kaliyappan, T.; Kannan, P. Studies on Twist Bent Core Zinc (II) Methacrylate Supramolecular Columnar Hexagonal Phase Mesogen derived from azobenzene moiety and its Photoluminescent Behaviours. *Inorg. Chem. Comm.* **2019**, *99*, 26–30. [CrossRef]
32. Morale, F.; Date, R.W.; Guillon, D.; Bruce, D.W.; Finn, R.L.; Wilson, C.; Blake, A.J.; Schröder, M.; Donnio, B. Columnar mesomorphism from hemi-disklike metallomesogens derived from 2,6-bis[3′,4′,5′-tri(alkoxy)phenyliminomethyl]pyridines (L): Crystal and molecular structures of [M(L)Cl_2 (M = Mn, Ni, Zn). *Chem. Eur. J.* **2003**, *9*, 2484–2501. [CrossRef] [PubMed]
33. Bhattacharjee, C.R.; Das, G.; Mondal, P.; Prasad, S.K.; Rao, D.S.S. Novel Green Light Emitting Nondiscoid Liquid Crystalline Zinc(II) Schiff-Base Complexes. *Eur. J. Inorg. Chem.* **2011**, *2011*, 1418–1424. [CrossRef]
34. Bhattacharjee, C.R.; Chakraborty, S.; Das, G.; Mondal, P. Emissive 'zinc(II)-salphen' core: Building block for columnar liquid crystals. *Liq. Cryst.* **2012**, *39*, 1435–1442. [CrossRef]
35. Cuerva, C.; Ovejero, P.; Campo, J.A.; Cano, M. Tetrahedral and octahedral metallomesogenic Zn(II) complexes supported by pyridine-functionalised pyrazole ligands. *New J. Chem.* **2014**, *38*, 511–517. [CrossRef]
36. Pucci, D.; Aiello, I.; Bellusci, A.; Crispini, A.; Ghedini, M.; La Deda, M. Coordination Induction of Nonlinear Molecular Shape in Mesomorphic and Luminescent ZnII Complexes Based on Salen-Like Frameworks. *Eur. J. Inorg. Chem.* **2009**, *2009*, 4274–4281. [CrossRef]
37. Ames, K.A.; Collinson, S.R.; Blake, A.J.; Wilson, C.; Love, J.B.; Bruce, D.W.; Donnio, B.; Guillon, D.; Schröder, M. Design of Neutral Metallomesogens from 5,5-Dimethyldipyrromethane: Metal Ion Mediated Control of Folding and Hairpin Structures. *Eur. J. Inorg. Chem.* **2008**, *2008*, 5056–5066. [CrossRef]
38. Giménez, R.; Manrique, A.B.; Uriel, S.; Barberá, J.; Serrano, J.L. Mesomorphism of a tetrahedral zinc complex. *Chem. Commun.* **2004**, *18*, 2064–2065. [CrossRef]
39. Chakraborty, S.; Bhattacharjee, C.R.; Mondal, P.; Prasad, S.K.; Rao, D.S.S. Synthesis and aggregation behaviour of luminescent mesomorphic zinc(II) complexes with 'salen' type asymmetric Schiff base ligand. *Dalton Trans.* **2015**, *44*, 7477–7488. [CrossRef]
40. Liu, Y.; Li, X.; Chen, J.; Yuan, C. Micro/Nano Electrode Array Sensors: Advances in Fabrication and Emerging Applications in Bioanalysis. *Front. Chem.* **2020**, *8*, 573865. [CrossRef]
41. Hannah, S.; Damion, E.B.; Corrigan, K. Developments in Micro and Nanoscale Sensors for Biomedical Sensing. *Curr. Opin. Electrochem.* **2020**, *23*, 7–15. [CrossRef]
42. Karimian, N.; Ugo, P. Recent advances in sensing and biosensing with arrays of nanoelectrodes. *Curr. Opin. Electrochem.* **2019**, *16*, 106–116. [CrossRef]
43. Yu, J.; Huang, T.; Jiang, Z.; Sun, M.; Tang, C. Synthesis and Characterizations of Zinc Oxide on Reduced Graphene Oxide for High Performance Electrocatalytic Reduction of Oxygen. *Molecules* **2018**, *23*, 3227. [CrossRef] [PubMed]
44. Sofianos, M.V.; Lee, J.; Silvester, D.S.; Samanta, P.K.; Paskevicius, M.; English, N.J.; Buckley, C.E. Diverse morphologies of zinc oxide nanoparticles and their electrocatalytic performance in hydrogen production. *J. Energy Chem.* **2020**, *56*, 162–170. [CrossRef]
45. Kelly, S.R.; Shi, X.; Back, S.; Vallez, L.; Park, S.Y.; Siahrostami, S.; Zheng, X.; Norskov, J.K. ZnO as an Active and Selective Catalyst for Electrochemical Water Oxidation to Hydrogen Peroxide. *ACS Catal.* **2019**, *9*, 4593–4599. [CrossRef]
46. Dayakar, T.; Rao, K.V.; Bikshalu, K.; Rajendar, V.; Park, S.H. Novel synthesis and structural analysis of zinc oxide nanoparticles for the non-enzymatic glucose biosensor. *Mater. Sci. Eng. C* **2017**, *75*, 1472–1479. [CrossRef]
47. Ramya, B.; Priya, P.G. Rapid phytochemical microwave-assisted synthesis of zinc oxide nano flakes with excellent electrocatalytic activity for non-enzymatic electrochemical sensing of uric acid. *J. Mater. Sci. Mater. Electron.* **2021**, *32*, 21406–21424. [CrossRef]
48. Motoc, S.; Cretu, C.; Costisor, O.; Baciu, A.; Manea, F.; Szerb, E.I. Cu(I) Coordination Complex Precursor for Randomized CuOx Microarray Loaded on Carbon Nanofiber with Excellent Electrocatalytic Performance for Electrochemical Glucose Detection. *Sensors* **2019**, *9*, 5353. [CrossRef]
49. Motoc, S.; Schinteie, B.; Pop, A.; Negrea, S.; Cretu, C.; Szerb, E.I.; Manea, F. Graphene Quantum Dots and Cu(I) Liquid Crystal for Advanced Electrochemical Detection of Doxorubicine in Aqueous Solutions. *Nanomaterials* **2021**, *11*, 2788. [CrossRef]
50. Szerb, E.I.; Pucci, D.; Crispini, A.; La Deda, M. Soft Luminescent Materials Based on Ag(I) Coordination Complexes. *Mol. Cryst. Liq. Cryst.* **2013**, *573*, 34–45. [CrossRef]
51. Pucci, D.; Barberio, G.; Bellusci, A.; Crispini, A.; Donnio, B.; Giorgini, L.; Ghedini, M.; La Deda, M.; Szerb, E.I. Silver Coordination Complexes as Room-Temperature Multifunctional Materials. *Chem. Eur. J.* **2006**, *12*, 6738–6747. [CrossRef] [PubMed]
52. The Cambridge Structural Database; Ma, Z.; Lu, W.; Liang, B.; Pombeiro, A.J.L. Synthesis, Characterization, Photoluminescent and Thermal Properties of Zinc(II) 4′-phenyl-terpyridine Compounds. *New J. Chem.* **2013**, *37*, 1529–1537. [CrossRef]

53. Soliman, A.B.; Abdel-Samad, H.S.; Abdel-Rehim, S.S.; Hassan, H.H. Surface functionality and electrochemical investigations of a graphitic electrode as a candidate for alkaline energy conversion and storage devices. *Sci. Rep.* **2016**, *6*, 22056. [CrossRef] [PubMed]
54. Elder, J.P. The Electrochemical Behavior of Zinc in Alkaline Media. *J. Electrochem. Soc.* **1969**, *116*, 757. [CrossRef]
55. Dumitru, C.-S.; Cojocaru, A.; Anicai, L.; Cotarta, A.; Visan, T. Electrodeposition of zinc oxide films from choline chloride based ionic liquid media containing zinc and nitrate ions. *UPB Sci. Bull. Ser. B* **2016**, *78*, 59.
56. Anwar, S.; Zhang, Y.; Khan, F. Electrochemical behaviour and analysis of Zn and Zn–Ni alloy anti-corrosive coatings deposited from citrate baths. *RSC Adv.* **2018**, *8*, 28861–28873. [CrossRef]
57. Renuka, R.; Srinivasan, L.; Ramamurthy, S.; Veluchamy, A.; Venkatakrishnan, N. Cyclic voltammetric study of zinc and zinc oxide electrodes in 5.3 M KOH. *J. Appl. Electrochem.* **2001**, *31*, 655–661. [CrossRef]